

# Water Resources Research

## RESEARCH ARTICLE

10.1029/2022WR031943

## Effects of Geologic Setting on Contaminant Transport in Deltaic Aquifers

Zhongyuan Xu<sup>1,2</sup>, Jayaram Hariharan<sup>3</sup> , Paola Passalacqua<sup>3</sup> , Elisabeth Steel<sup>4</sup>, Austin Chadwick<sup>5</sup> , Chris Paola<sup>5</sup> , Anner Paldor<sup>2</sup> , and Holly A. Michael<sup>2,6</sup> 

<sup>1</sup>Faculty of Geosciences and Environmental Engineering, Southwest Jiaotong University, Chengdu, China, <sup>2</sup>Department of Earth Sciences, University of Delaware, Newark, DE, USA, <sup>3</sup>Department of Civil, Architectural and Environmental Engineering, Center for Water and the Environment, University of Texas at Austin, Austin, TX, USA, <sup>4</sup>Department of Geological Sciences and Geological Engineering, Queen's University, Kingston, ON, Canada, <sup>5</sup>St. Anthony Falls Laboratory, Department of Earth and Environmental Sciences, University of Minnesota, Minneapolis, MN, USA, <sup>6</sup>Department of Civil and Environmental Engineering, University of Delaware, Newark, DE, USA

### Key Points:

- In deltaic aquifers, contaminant distribution is controlled by the sand fraction and channel stacking patterns
- Rivers on the surface have a strong influence on vertical contaminant transport in aquifers
- Due to differences in channel distribution, vertical contamination varies nonlinearly from upstream to downstream regions

### Supporting Information:

Supporting Information may be found in the online version of this article.

### Correspondence to:

H. A. Michael,  
[hmichael@udel.edu](mailto:hmichael@udel.edu)

### Citation:

Xu, Z., Hariharan, J., Passalacqua, P., Steel, E., Chadwick, A., Paola, C., et al. (2022). Effects of geologic setting on contaminant transport in deltaic aquifers. *Water Resources Research*, 58, e2022WR031943. <https://doi.org/10.1029/2022WR031943>

Received 5 JAN 2022  
Accepted 19 AUG 2022

**Abstract** Coastal deltaic aquifers are vulnerable to degradation from seawater intrusion, geogenic and anthropogenic contamination, and groundwater abstraction. The distribution and transport of contaminants are highly dependent on the subsurface sedimentary architecture, such as the presence of channelized features that preferentially conduct flow. Surface deposition changes in response to sea-level rise (SLR) and sediment supply, but it remains unclear how these surface changes affect the distribution and transport of groundwater solutes in aquifers. Here, we explore the influence of SLR and sediment supply on aquifer heterogeneity and resulting effects on contaminant transport. We use realizations of subsurface heterogeneity generated by a process-based numerical model, DeltaRCM, which simulates the evolution of a deltaic aquifer with different input sand fractions and rates of SLR. We simulate groundwater flow and solute transport through these deposits in three contamination scenarios: (a) vertical transport from widespread contamination at the land surface, (b) vertical transport from river water infiltration, and (c) lateral seawater intrusion. The simulations show that the vulnerability of deltaic aquifers to seawater intrusion correlates to sand fraction, while vertical transport of contaminants, such as widespread shallow contamination and river water infiltration, is influenced by channel stacking patterns. This analysis provides new insights into the connection between the depositional system properties and vulnerability to different modes of groundwater contamination. It also illustrates how vulnerability may vary locally within a delta due to depositional differences. Results suggest that groundwater management strategies may be improved by considering surface features, location within the delta, and the external forcings during aquifer deposition.

**Plain Language Summary** The findings of this study provide insight into the vulnerability of deltaic aquifers to three contamination processes: (a) widespread contaminant transport from the land surface, (b) river water infiltration, and (c) seawater intrusion. We consider how contamination is affected by the location of contaminants and the processes associated with the accumulation of sediments in deltas. Our work shows that vulnerability to contamination depends on how the aquifer is deposited. The results also demonstrate that the distribution of sandy channels preserved in the subsurface, as well as rivers on the surface, controls vertical contaminant transport. We find that these effects vary from upstream to downstream in the delta because of spatial differences in depositional processes. These findings will help to improve predictions of groundwater contamination and manage groundwater development in deltas around the world.

## 1. Introduction

Deltaic aquifers and river basins provide water resources to over 300 million people globally (Edmonds et al., 2020; Giosan et al., 2014; Syvitski & Saito, 2007). Groundwater is often the primary source for water supply due to the high uncertainty of availability and typically low quality of surface water (Shamsudduha et al., 2011). However, fresh groundwater resources in deltas are threatened by multiple onshore and offshore contaminants (Hosono et al., 2011; Michael & Voss, 2008; Nofal et al., 2015; Vetrimurugan et al., 2013). Aquifer salinization and geogenic arsenic are two major issues (Ayers et al., 2016); in mega deltas of Southern Asia alone, >25 million people and >100 million people are at risk of drinking saline water (Shammi et al., 2019) and high-arsenic water, respectively (Fendorf et al., 2010; Ng et al., 2003; WHO, 2011). The vulnerability of uncontaminated deltaic

aquifers to the migration of these and other contaminants is strongly tied to the subsurface sedimentary structure, which results from depositional processes. Despite its importance, knowledge of subsurface structure is always limited by scarcity of in-situ data. Building a full understanding of the links between contaminant transport processes and depositional processes is therefore critical to improving the sustainability of groundwater resources in deltaic settings.

Groundwater flow in heterogeneous fields can be dominated by preferential flow pathways, resulting in anomalous solute transport that is not well simulated by the classical Fickian advection-dispersion model (Berkowitz et al., 2000; Carrera, 1993; Feehley et al., 2000; Rubin, 1991). Connected features have recently received attention because they have substantial effects on flow and transport and they are difficult to capture in models of heterogeneity simulated with classical geostatistical methods (Wen & Gomez-Hernandez, 1998; Western et al., 2001; Zinn & Harvey, 2003). Connected high-permeability features produce fast-flow channeling and significantly reduce contaminant arrival times (Fiori & Jankovic, 2012; Knudby & Carrera, 2005; Le Goc et al., 2010). Deltaic aquifers have a similar subsurface structure with sand-rich paleo-channels and high variability in permeability (Kolker et al., 2013).

Aquifer salinization can be caused by lateral seawater intrusion (Bear, 1999; Henry, 1964; Michael et al., 2013; Werner & Simmons, 2009; Werner et al., 2013) and vertical infiltration of seawater due to storm surges and flooding (Anderson, 2002; Holding & Allen, 2015; Yang et al., 2015b; Yu et al., 2016). Lateral seawater intrusion in coastal aquifers is significantly influenced by geologic heterogeneity (Werner et al., 2013), which controls the slope and width of freshwater-seawater mixing zones (Cameo, 2006; Lu et al., 2013), enhances groundwater circulation driven by salinity gradients (Kaleris, 2006; Kerrou & Renard, 2009), and produces complex subsurface salinity distributions that can extend tens of kilometers offshore (Michael et al., 2016). Furthermore, in highly heterogeneous coastal aquifers, the network of connected features exerts a significant effect on freshwater-seawater interaction and nearshore groundwater flow, including fractured coastal aquifers (Sebben et al., 2015), coastal karst aquifers (Xu et al., 2019), coastal aquifers with lava tubes (Kreyns et al., 2020), and deltaic aquifers with paleo-channels (Mulligan et al., 2007; Rao et al., 2005). Fast seawater intrusion through preferential flow paths is enhanced by pumping, resulting in much higher vulnerability compared to more homogeneous systems (Geng & Michael, 2020; Yu & Michael, 2019).

Lateral seawater intrusion has been studied for decades, whereas fewer researchers have investigated vertical seawater infiltration. However, vertical salt infiltration during coastal inundation is a greater concern for aquifer salinization than lateral seawater intrusion (Taylor et al., 2013; Yu, 2010). Subsurface properties primarily influence both the occurrence and time to flush salt out of the aquifer. Yang et al. (2018) investigated the effects of hydrogeologic factors (permeability, hydraulic gradient, and recharge rate) on salinization in homogeneous systems and showed that anisotropy in permeability has a strong effect. This anisotropy is an upscaled effect of the small-scale heterogeneous permeability distribution. Climate change has also been shown to impact seawater infiltration (Yang et al., 2015a, 2015b). Vithanage et al. (2012) used laboratory experiments and numerical simulations to study groundwater salinization from tsunamis in heterogeneous media, and they showed that geologic heterogeneity influenced flushing times. Sawyer et al. (2015) showed that delta morphology has an important impact on surface water—groundwater interactions and influences solute transport after flooding. Yu et al. (2016) analyzed the impact of mesoscale topography on seawater infiltration and concluded that landscape features, such as connected surface water conduits, are a primary indicator of coastal groundwater vulnerability.

Widespread, naturally occurring arsenic is another common groundwater pollutant in deltas, particularly in Southern Asia (e.g., Berg et al., 2007; Fendorf et al., 2010). High arsenic in these aquifers occurs primarily within shallow Holocene sediments (<100 m depth), but it can migrate downward to contaminate deeper strata due to natural processes (Khan et al., 2019) and groundwater overdevelopment (Erban et al., 2013; Khan et al., 2016; Michael & Voss, 2008). Several studies have shown the importance of geologic heterogeneity in controlling arsenic transport. Hoque et al. (2017) explained arsenic distributions in the Bengal Delta, Bangladesh with a discontinuous silt-clay model. Mozumder et al. (2020) used detailed site-specific lithologic and geochemical data to show that groundwater pumping in the megacity Dhaka, Bangladesh and aquifer structure control arsenic migration from shallow (<40 m) to intermediate (40–90 m) aquifer depths. Khan et al. (2016) and Michael and Khan (2016) used geostatistical representations of aquifer heterogeneity to show that deep (>150 m), low-arsenic groundwater in the Bengal Delta is threatened by preferential transport under pumping.

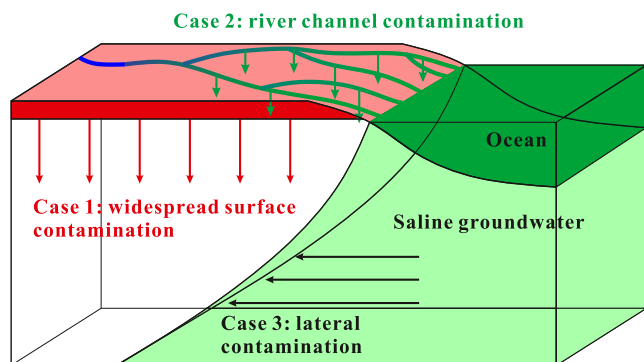


**Figure 1.** The conceptual model of three contamination scenarios. Case 1 is widespread surface contamination (representing shallow arsenic contamination), Case 2 is river channel contamination (representing infiltration of seawater from surface channels into the subsurface), and Case 3 is lateral contamination (representing subsurface seawater intrusion).

While these studies clearly show the important controls of heterogeneity on arsenic transport and contaminant vulnerability, most do not consider continuous channel structures. Deltaic subsurface architecture contains paleo-channels that are created through the evolution of the surface system (Liang et al., 2016). Paleo-channels were deposited by river channels, which migrate and redistribute sediment over time. These subsurface channels stack in a sequence dependent on river evolution (Hiatt & Passalacqua, 2015; Reitz et al., 2015; Shaw, 2013). This active sediment deposition is controlled by environmental forcings, such as sea-level change and sediment grain size (Heller et al., 2001; Sheets et al., 2002). The connectivity of sand-rich paleo-channels and stacking of paleo-channel networks control the groundwater flow in horizontal and vertical directions (Xu et al., 2021); thus, a better understanding of how external forcings during deposition create the features that control solute transport can substantially improve our ability to predict vulnerability in deltaic environments.

In this study, we use DeltaRCM (Liang et al., 2015) to simulate delta evolution, producing both surface topography and realistic subsurface heterogeneity that includes stacked paleochannels. Different external forcings during

deposition are applied when generating delta models. Three scenarios of contaminant transport are considered: Case 1—widespread surface contamination, Case 2—river channel contamination, and Case 3—lateral contamination. These three cases conceptually represent vertical arsenic transport, seawater infiltration from river channels and lateral seawater intrusion, respectively (Figure 1).

## 2. Methods

### 2.1. Geologic Models of Deltaic Aquifers

The channelized heterogeneous models (Figure 2a) of delta aquifers were generated with DeltaRCM (Liang et al., 2015). DeltaRCM is a process-based model that simulates deltaic evolution through the water-mediated transport of sediment and records depositional processes over time. Randomness in the DeltaRCM model is due to the simulation of reduced complexity hydrodynamics and sediment transport using weighted random walks. Walk weights are regulated by physical rules such as water surface slope, water depth, and velocity. The total extent of DeltaRCM models is roughly 4,000 m in the longitudinal direction, which is the direction aligned with the inlet channel, 10,000 m in the traverse direction and 50 m in the vertical direction. The models were discretized into cuboid cells with dimensions of 50 m (longitudinal)  $\times$  50 m (traverse)  $\times$  5 cm (vertical), which is the same as in previous studies using DeltaRCM models (Liang et al., 2015, 2016) (Figure 2a, Text S1 in Supporting Information S1). DeltaRCM records the sand fraction in each cell, from 0 (pure mud) to 1 (pure sand). The term mud is used here for simplicity, representing a mixture of low-permeability silt and clay.

In this study, two external forcing factors were considered in the delta evolution process: input sand fraction (ISF) and the rate of sea-level rise (SLR). ISF is the fraction of coarse sediment that is introduced at the inlet, which determines the total sand input to the delta and strongly influences the sand content of each cell as well as system kinematics and sand distribution (Liang et al., 2015, 2016). Several studies showed that sandy deltas (higher ISF) have shallower river channels, a larger number of islands, and more active channel migration compared to muddier ones (Edmonds et al., 2011; Hoyal & Sheets, 2009; Liang et al., 2016; Sawyer et al., 2015). ISF values of 30%, 50%, and 70% were used in this study to cover the range of most delta types. SLR is another critical factor influencing delta morphodynamics; higher SLR results in more channel distributaries and a higher aggradation rate, resulting in a thicker and narrower delta (Liang et al., 2016). To obtain robust results for vertical transport, the groundwater modeling analysis requires deltas that are thick enough to contain multiple stacked channel features. In order to create such models in a computationally reasonable time period, very large values of SLR were used, 40, 50, and 60 mm/yr (see Section 4.2 for more details). All models were simulated for 500 yr for delta growth with the assumption of 10 bankfull days per year, and further delta growth during the groundwater simulation was neglected. Based on model population tests, eight models are sufficient for data analysis in this study (Text S2 and Figure S1 in Supporting Information S1). Overall, 8 realizations for each of 3 ISF and 3 SLR values were generated, resulting in 72 synthetic deltas.

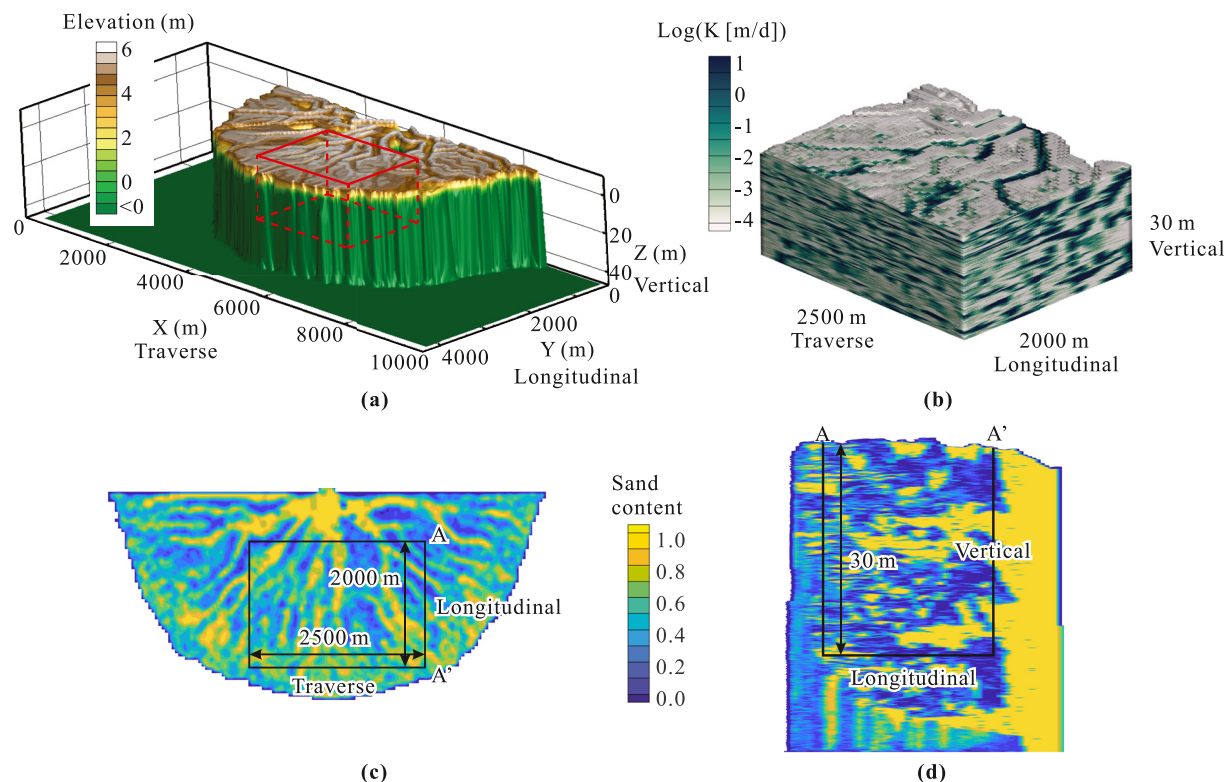


**Figure 2.** Geological and groundwater models. (a) Model generated by DeltaRCM. Red box shows the extracted portion for the groundwater model. (b) Hydraulic conductivity ( $K$ ) in the extracted domain (red box shown in panel (a)), based on the sand content. (c) Plan view of the groundwater model outlined on the geologic model. (d) Side view of groundwater model outlined on the geologic model.

## 2.2. Model Setup

The groundwater models are cuboid boxes cut from the DeltaRCM geologic models (Figure 2 and Text S1 in Supporting Information S1). The boxes exclude the high sand content at the inlet to maximize statistical stationarity, though trends still exist (i.e., distal fining and channel thinning). The models are 2,000 m (longitudinal)  $\times$  2,500 m (transverse)  $\times$  30 m (vertical) with 1.2 million cells, although some cells are inactive on the top since they were eroded by river channels. The sand content of each cell was converted to hydraulic conductivity ( $K$ ), assigning to pure mud a value of  $1 \times 10^{-9}$  m/s and to pure sand a value of  $1 \times 10^{-4}$  m/s. The  $K$  of a cell that contains a mixture of sand and mud was calculated as the geometric mean based on the sand content value in this cell by the same method as Xu et al. (2021). Groundwater flow and advective-dispersive solute transport were simulated with MODFLOW (Harbaugh, 2005), MT3DMS (Zheng & Wang, 1999), and SEAWAT (Langevin et al., 2008) (Case 3 only, see below). The porosity was 0.4 for both materials to keep the transport solution consistent, and the horizontal and vertical dispersivity were 100 and 0.5 m, respectively. The same realizations were used in three cases of contaminant transport. The illustrations and boundary conditions of the three cases are shown in Figure 3 and explained below. While we frame the three cases as common contamination scenarios in deltas (salt and arsenic, movement induced by pumping), we discuss the solute transport in general terms and consider only conservative transport.

The three transport cases include two cases of a general contaminant (e.g., arsenic) and a third case of salinization due to saltwater intrusion. Solute concentrations are simulated as relative values ( $0 \leq C \leq 1$ ). For Case 3a, steady state lateral salinization, a variable-density component is added to the flow, which requires a specific salinity value for the maximum concentration ( $C = 1$ ) associated with a maximum density. That maximum salinity (equal to seawater) was taken as 35 g/L, corresponding to a density of 1,025 kg/m<sup>3</sup>.

Case 1 consists of a consistent source of contamination all along the land surface (red in Figure 1). This scenario is based on widespread shallow arsenic contamination in the deltas of Southern Asia (e.g., Fendorf et al., 2010). Downward arsenic transport occurs when groundwater flows from shallow to deep aquifers, driven by hydraulic

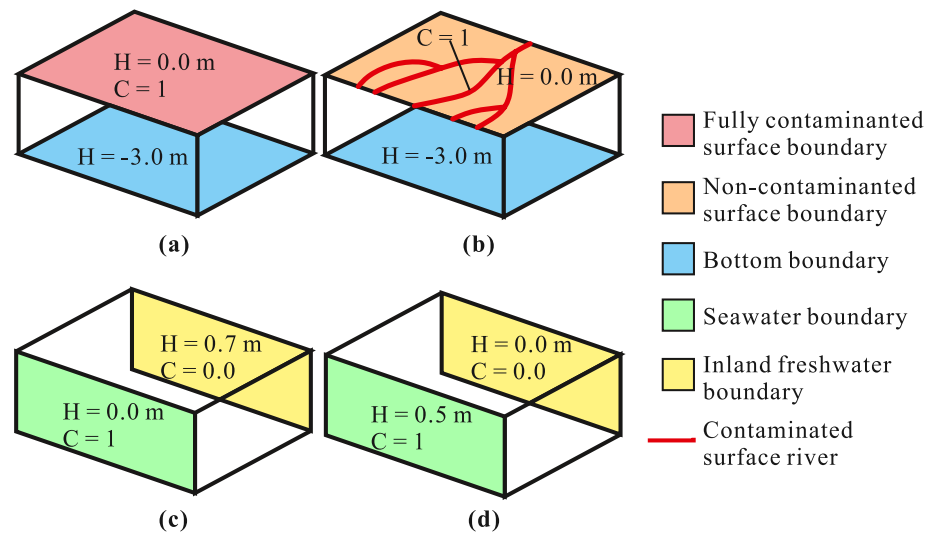


**Figure 3.** The boundary conditions for the three contamination cases. (a) Case 1, (b) Case 2, (c) Case 3a steady state, (d) Case 3b seawater intrusion.

gradients caused by pumping (e.g., Khan et al., 2016; Radloff et al., 2011). In this study, transient solute transport was simulated with MODFLOW and MT3DMS. Constant-head boundaries were applied on the surface ( $H = 0$  m) and bottom ( $H = -3$  m) of the model. The head difference was 3 m to indirectly simulate the groundwater pumping effect and all other boundaries are no flow (Figure 3a). Transport boundary conditions were a constant concentration of  $C = 1$  on the entire land surface (Figure 3a) and a zero concentration gradient boundary on the bottom, the simulation time was 200 yr. This case is designed to test the effects of heterogeneity on vertical transport of widespread surface contamination.

Case 2 consists of a contaminant source only along surface river channels, representing a scenario of vertical infiltration of salt or other contaminants from surface rivers to groundwater (green in Figure 1). Due to flat topography and tidal forcing, seawater intrusion into river channels is a common problem in deltas (Bricheno & Wolf, 2018). Contaminants in the river could be a source of pollution to groundwater, particularly if groundwater pumping is drawing surface water into the aquifer. In this scenario, a constant concentration boundary was assigned along the surface river channels ( $C = 1$ ) and nonriver region ( $C = 0$ ), the bottom is a zero concentration gradient condition for solute transport. The flow boundary conditions were the same as in Case 1 (Figure 3b). MODFLOW was used to calculate the steady state groundwater flow, MT3DMS was used to simulate advective-dispersive transport for 200 yr. This scenario is designed to test the effects of heterogeneity on vertical transport as in Case 1, but particularly considers connectivity between channels and the subsurface (i.e., Case 2 and Case 1 will be similar if channel stacking is less persistent, and more dissimilar if channels tend to build in the same place over time). To be able to directly compare Case 1 and Case 2, we did not incorporate variable-density flow into Case 2, which would occur for the intrusion of brackish surface water into fresh groundwater.

Case 3 consists of a consistent source of contamination on one vertical side of the domain based on the scenario of lateral seawater intrusion (black arrows in Figure 1). We considered two sub-cases, one (Case 3a) consists of the salinity distribution and associated density-driven saline groundwater circulation under steady state conditions. The second sub-case (Case 3b) consists of transient seawater intrusion due to sea-level rise. We considered these two subcases because density-driven groundwater flow (Case 3a) causes rotational convection within the seawater wedge, which is influenced by both horizontal and vertical connectivity. Thus, the rotational flow is intermediate between the fully vertical (Case 1 and Case 2) and fully horizontal (Case 3b) transport scenarios. We neglected density effects in Case 3b so that fully horizontal transport can be compared directly to fully vertical transport in Case 1 and Case 2. In the sub-case of steady-state conditions (Case 3a), numerical models were developed in SEAWAT to simulate the density-dependent groundwater flow and salt transport, and the simulation was run until the system (groundwater flow and salinity distributions) reached steady state. Constant head and constant salinity were applied on the seaside and freshwater boundaries, while other faces, including the delta surface, are no-flow boundaries. The inland hydraulic head was 0.7 m higher than sea level. The constant

**Table 1**  
*The Definition of Groundwater Contamination Assessment Indicators*

Metric	Case	Definition
Largest depth of contamination	1 and 2	The largest depth of the $C = 1$ contour in the vertical movement of contaminant (Figure 5a)
Average depth of contamination	1 and 2	The mean depth of the $C = 1$ contour in the vertical movement of contaminant (Figure 5a)
Transport connectivity <sup>a</sup>	1	Largest depth of contamination (the $C = 1$ contour) divided by average depth of contamination
Solute mass per unit area	1 and 2	The total mass of contaminant in the system divided by the surface contaminated area. The concentration values were normalized to unitless 0–1, this metric is concentration (unitless) $\times$ volume(m <sup>3</sup> )/area(m <sup>2</sup> ), the unit is m
Variance in transport depth	1	The variance of depth of the $C = 1$ contour in the vertical movement of contaminant
Saline groundwater volume	3a	The volume of aquifer with solute concentration greater than 0.0143 (Figure 5b)
Landward position of interface toe	3a	The distance between the freshwater-saltwater interface ( $C = 0.0143$ ) at the model bottom to the seaward boundary (Figure 5b)
Saline SGD	3a	The rate of saltwater discharge at the seawater boundary
Fresh SGD	3a	The rate of freshwater discharge at the seawater boundary
Ratio of saline to fresh SGD	3a	Saline SGD divided by Fresh SGD
Salinized volume	3b	The volume of aquifer with $C > 0.0143$ after solute transport for 200 yr (Figure 5c)
Farthest seawater extent	3b	The most landward location of the $C = 0.0143$ contour after solute transport 200 yr (Figure 5c)

<sup>a</sup>Both flow and transport connectivity consider the bulk fluid behavior versus preferential behavior. The difference between flow and transport connectivity is how they are calculated, such as  $K_{eff}/K_G$  (effective hydraulic conductivity normalized by geometric mean of conductivity) and  $T_d/T_5$  (Average transport time of tracked particles normalized by transport time of the fastest fifth percentile of particles) used in Xu et al., 2021. In this study, we used the solute transport distance, in which the largest contaminant depth represents preferential behavior and the average contaminant depth represents bulk behavior.

concentration was  $C = 1$  (representing a salinity of 35 g/L) and  $C = 0$  (0 g/L) at the sea boundary and inland boundary, respectively (Figure 3c). The sub-case of seawater intrusion (Case 3b) tests the effect of heterogeneity on horizontal contamination. Simulations were run for 1,000 yr without a density effect so that the case could be compared more directly to Case 1 and Case 2. For this case, the sea level (seaward boundary head) was 0.5 m higher than the inland hydraulic head, which represents conditions of aquifer pumping or sea-level rise. The other boundary conditions were the same as the steady-state case (Figure 3d).

Another important feature of the models is topography. Since the models were randomly generated by DeltaRCM, the topography of each realization is different. One important factor that influences contaminant transport is the location of surface rivers because they determine the location and extent of contaminant sources for Case 2. We consider surface pixels in the DeltaRCM model to be rivers that have a surface flow rate greater than 0.3 m/s (Liang et al., 2015). Figure S2b in Supporting Information S1 shows the ratio of surface river area to the total surface area for the different ISF and SLR realizations. The proportion of model surface classified as river channels ranges from 0.2 to 0.6 and slightly increases with ISF and SLR. The comparison of Case 1 and Case 2 was used to analyze the effect of surface rivers, exploring whether surface channel networks are more connected to the subsurface than other locations on land surface.

### 2.3. Groundwater Contamination Assessment Indicators

To quantify the extent of solute transport in each scenario, 12 indicators were calculated (Table 1). The contaminant volume or distance in the following indicators refer to the value at the end of simulation. For Cases 1 and 2, metrics were chosen to quantify contaminant mass input and vertical travel distance. The depth of contamination was quantified as the distance from the surface to the deepest location where solute concentration equals 1 along

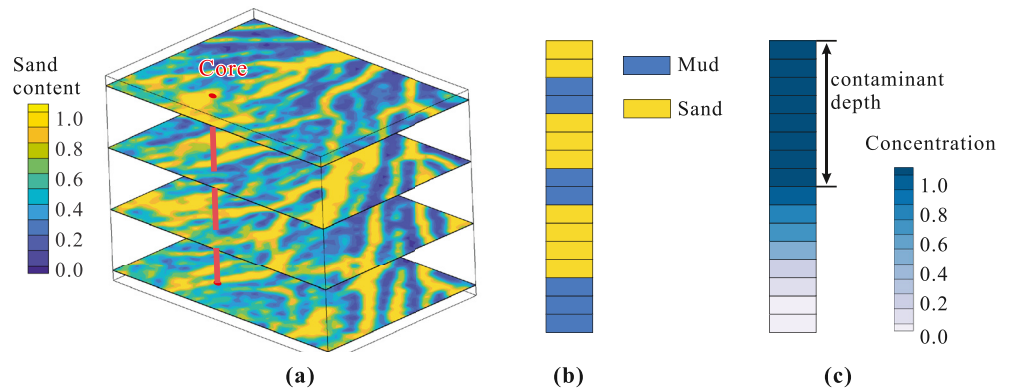


**Figure 4.** (a) A core in the system (red line), defined as the column of all cells that are aligned vertically at a given horizontal location. (b) An illustrative example of a sand-mud distribution of modeled cores. In the example core shown in panel (b), the *sand package connectivity* is 0.44 (largest group is 4 out of 9 total sand cells, see Table 2), and the *number of sand-mud transitions* is 5. Panel (c) is the vertical concentration profile of the core in panel (a), as simulated by the groundwater model. In panel (c), the contaminant depth is about half of the core length.

each core in Figure 4c. The *largest depth of contamination*, *average depth of contamination*, *solute mass per unit area* and *variance in transport depth* were calculated to measure vertical contamination (Table 1, Figure 5a). For Case 3a, *saline groundwater volume*, *landward position of interface toe*, *saline SGD* (Submarine groundwater discharge), *fresh SGD*, and *ratio of saline to fresh SGD* were calculated to measure density-dependent contamination (Table 1, Figure 5b). For Case 3b, the *salinized volume* and *farthest seawater extent* were calculated to measure horizontal contamination (Table 1, Figure 5c).

#### 2.4. Static Indicators

Previous research demonstrated that groundwater flow is controlled by geologic structure (Xu et al., 2021). To better explain how the sediment distribution influences contamination, especially variation from upstream to downstream, it is necessary to use static metrics to quantify the connectivity of geologic properties (Knudby & Carrera, 2005; Renard & Allard, 2013). In this study, we focus on sand distribution and channel stacking, and three static metrics are defined (Table 2): *Sand fraction*, *sand package connectivity*, and *number of sand-mud transitions*. *Sand fraction* has been shown to correlate well with lateral flow behavior (Xu et al., 2021); we note that *Sand fraction* is different from ISF because it is measured on the sampled groundwater domain. *Sand package connectivity* and the *number of sand-mud transitions* are calculated on cores in the model (Figure 4b), which are vertical columns under each cell in the X-Y direction (Table 2). *Sand package connectivity* measures vertical connectivity and is an indicator of channel stacking. The *number of sand-mud transitions* reflects variability in the depositional environment and channel migration.

We further used Analysis of Variance tests (ANOVA) to statistically compare both static and dynamic indicators among different simulated scenarios. ANOVA test is able to analyze the differences among groups of data, the *p*-values of ANOVA tests less than 0.05 indicate that differences in transport behavior are statistically significant.

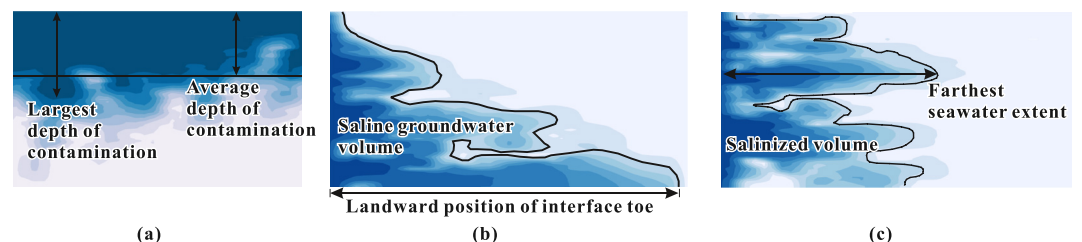


**Figure 5.** Illustration of the metrics for the three contamination cases. (a) Case 1 and Case 2. (b) Case 3a. (c) Case 3b. Black contours in panels (b) and (c) are  $C = 0.0143$ .

**Table 2**  
The Definition of Static Indicators

Metric	Definition
Sand fraction	The average sand content of all cells in the domain
Sand package connectivity	The ratio of the largest group of sand cells (sand content $\geq 0.8$ ) to the total volume of sand cells in cores (Hariharan et al., 2021, Figure 4b)
Number of sand-mud transitions	The number of shifts from sand (sand content $\geq 0.8$ ) to mud (sand content $< 0.8$ ) and from mud to sand in cores (Figure 4b)

### 3. Results

Simulated solute distributions show the influence of geologic heterogeneity in all three contamination cases (Figure 6). The influence of ISF and SLR on stratigraphic and solute transport indicators is discussed below.

#### 3.1. Surface Source of Contamination, Vertical Transport

**Case 1.** Vertical solute transport from the land surface is highly influenced by ISF and SLR (Figure 7). The *average depth of contamination* increases from 1.8 m for 30% ISF to 3.5 m for 70% ISF (Figure 7a), with an especially rapid increase between 50% and 70% ISF. The effect of SLR is different for different values of ISF. For 30% and 50% ISF, the *average depth of contamination* decreases with SLR, most likely because the sand fraction in the model domain decreases with SLR (Figure S2a in Supporting Information S1; Xu et al., 2021). *Average depth of contamination* increases with SLR in 70% ISF realizations, most likely due to higher rates of channel migration in very sandy deltas that promote more vertical sand connections. This result shows that both ISF and SLR affect transport and connectivity (see also Hariharan et al., 2021). The *solute mass per unit area* varies similarly to the *average depth of contamination*, increasing with ISF from 3 to 10 m and decreasing with SLR under 30% and 50% ISF conditions (Figure 7b).

The *largest depth of contamination* is an indicator of preferential transport behavior (Figure 7c). There is not a significant trend in this metric with external forcings, the average values range from 15 to 20 m, and the greatest

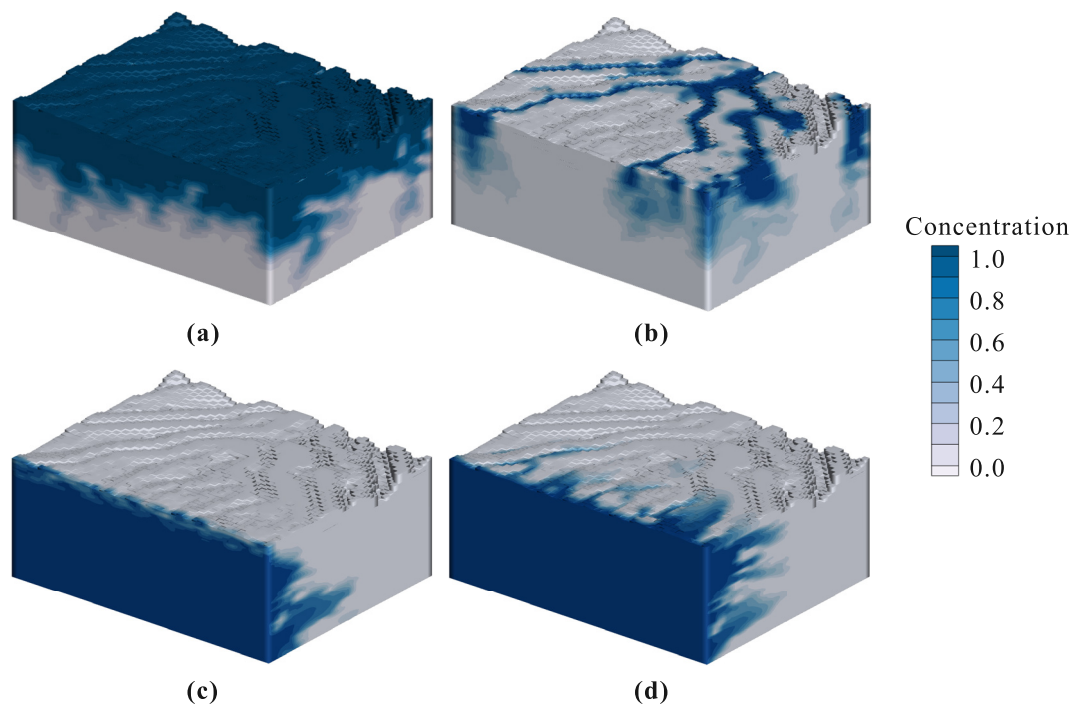


**Figure 6.** Example solute distributions (normalized concentration) for the three contamination cases. (a) Case 1 (simulation time 200 yr) and (b) Case 2 (simulation time 200 yr). (c) Case 3a (steady state) and (d) Case 3b seawater intrusion (simulation time 1,000 yr).

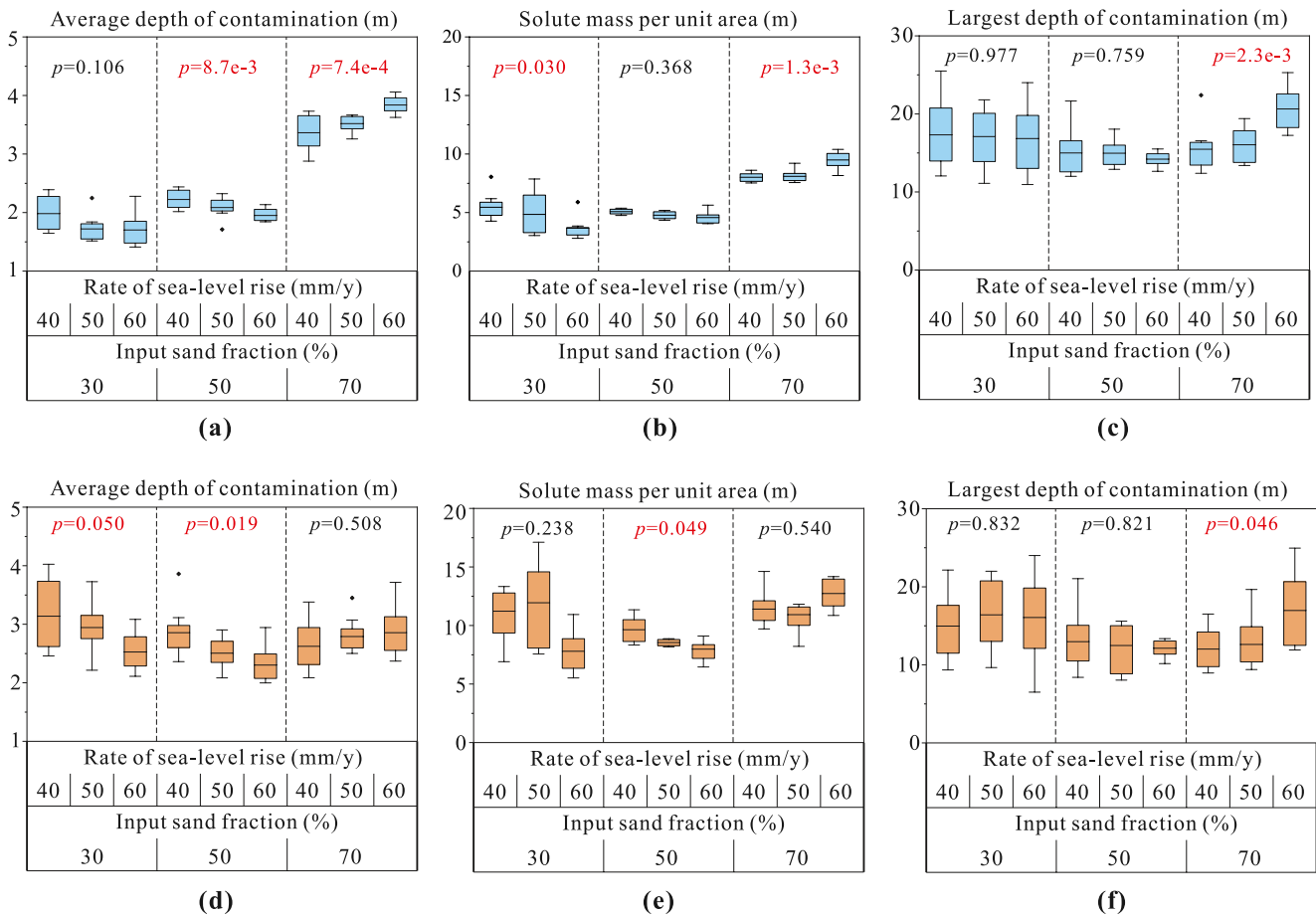


**Figure 7.** Results of contaminant transport simulations for Case 1 and Case 2. Panels (a–c) are widespread surface contamination (Case 1). Panels (d–f) are surface river channel contamination (Case 2). The  $p$ -values of Analysis of Variance tests are displayed in each input sand fraction (ISF) group,  $p$ -values less than 0.05 indicate that the differences in transport behavior are statistically significant. Rate of sea-level rise (SLR) and ISF are parameters in the delta evolution process, not the solute transport simulation.

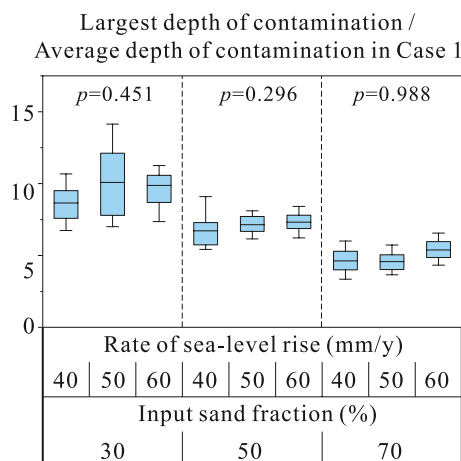


**Figure 8.** The ratio of the largest depth of contamination to average depth of contamination in Case 1. The  $p$ -values of the Analysis of Variance tests are displayed in each input sand fraction (ISF) group,  $p$ -values less than 0.05 indicate that the differences in transport behavior are statistically significant. Rate of sea-level rise (SLR) and ISF are parameters in the delta evolution process, not the sol transport simulation.

depths reach more than 25 m. The contamination depth in 30% ISF realizations is deeper than in 50% and 70% ISF models in some cases, likely because river channels in muddier deltas (lower ISF) are more persistent than in sandy deltas, creating more vertical connectivity. This illustrates that the vulnerability of deltas to arsenic contamination cannot be predicted by sand fraction alone, since channel migration is another important factor controlling vertical transport.

Furthermore, we defined a metric of *transport connectivity* as the *largest depth of contamination* normalized by an *average depth of contamination*, which effectively measures preferential transport that results in a maximum contamination depth greater than the average contamination depth (Table 1). This normalized metric allows comparison of the preferential nature of flow across aquifers with different sand fractions (see, e.g., Hariharan et al., 2021; Xu et al., 2021). *Transport connectivity* decreases with ISF, indicating a smaller difference between the *largest depth of contamination* and an *average depth of contamination* in models with higher sand fraction (Figure 8). Higher sand fraction results in more connected fast flow pathways throughout the aquifer, substantially increasing the average depth of contamination while not obviously contributing to the *largest depth of contamination*. However, more active channel migration induced by increased ISF inhibits the *largest*

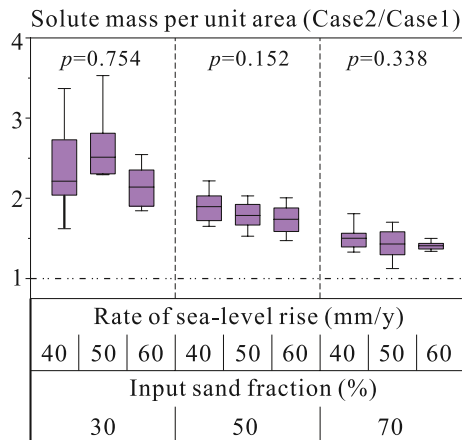


**Figure 9.** The ratio of solute mass per unit area, from Case 2 to Case 1. The  $p$ -values of the Analysis of Variance tests are displayed in each input sand fraction (ISF) group,  $p$ -values less than 0.05 indicate that the differences in transport behavior are statistically significant. Rate of sea-level rise (SLR) and ISF are parameters in the delta evolution process, not the sol transport simulation.

*depth of contamination.* This conclusion is similar to the previous study of flow connectivity in deltaic aquifers (Xu et al., 2021): vertical flow connectivity ( $K_{\text{eff}}/K_G$ ) and transport connectivity ( $T_a/T_s$ ) decrease with sand fraction.

**Case 2.** The contaminated water infiltrating into the aquifer from surface river channels is not strongly influenced by ISF. The *average depth of contamination* in Case 2 ranges from 2 to 4 m for 30%–70% ISF conditions, with no significant trend with ISF (Figure 7d). Trends with SLR show that an *average depth of contamination* decreases with higher rates of SLR in the 30% and 50% ISF groups and increases with higher rates of SLR in the 70% ISF group. The *solute mass per unit area* (the mass of solute infiltrated divided by the area of the land surface) also does not vary substantially with ISF and ranges from 5 to 17 m (Figure 7e).

**Case 1 and Case 2 Comparison.** The differences between Case 1 and Case 2 indicate the extent to which modern surface channels are more connected to the subsurface than other areas of land surface. The effect of ISF in Case 2 is weaker than in Case 1 (compare Figure 7) since the channel migration is not strongly controlled by the ISF. The *largest depth of contamination* in Case 2 is similar to that in Case 1 (Figures 7c and 7f) because in both cases, the deepest transport occurs in sandy channels connected to surface channels. If the deepest transport in Case 2 is the same as in Case 1, it would indicate that the fastest transport pathways are connected to surface channels. In general, the transport behavior of Case 2 is less dependent on sand fraction than Case 1.

The distribution and area of surface river channels are important factors for vertical contaminant transport because channels are more likely to be connected to subsurface sandy channels than non-channel regions. To quantify the effect of river channels on vertical transport, the ratio of solute mass per unit area for Case 2/Case 1 was calculated. Figure 9 shows that ratios under all external forcings are  $>1$ , which means that river channels contribute more contaminants to the aquifers than nonriver regions. However, this ratio decreases with ISF, indicating that the effect of surface rivers becomes weaker as systems become sandier. In sandy deltas, the subsurface sandy channels are wider and more variable, and contaminants from nonriver regions may also be well connected to sandy channels.

**Spatial variation from upstream to downstream** is another important factor that influences contaminant distributions in deltas. Typically, there are fewer, larger channels in the upstream area that develop into multiple distributaries downstream. This creates channel stacking patterns and connectivity that vary from upstream to downstream. Figure 10a shows the difference in sand distributions between upstream and downstream cross-sections. To quantify these spatial variations, both static indicators and contamination indicators were calculated in subregions comprising 40 2-dimensional vertical bands with 50 m intervals in radius from the sediment source (Figure 10b).

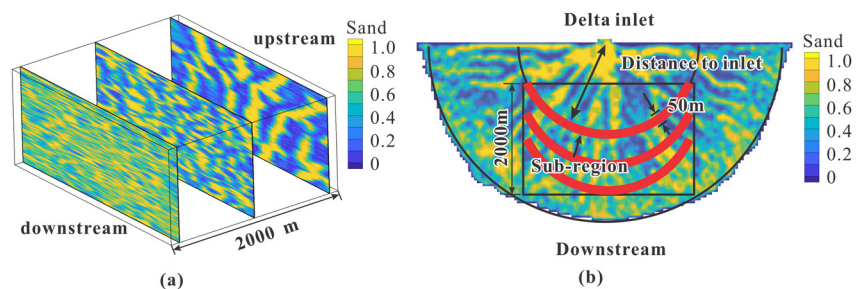


**Figure 10.** (a) Sand distributions in subregions of the model from upstream to downstream. (b) Subregions are defined as circular arcs along an equal distance from the inlet, with 50 m intervals. Since the sand distribution varied along the 40 subregions, static metrics were measured for each subregion separately.

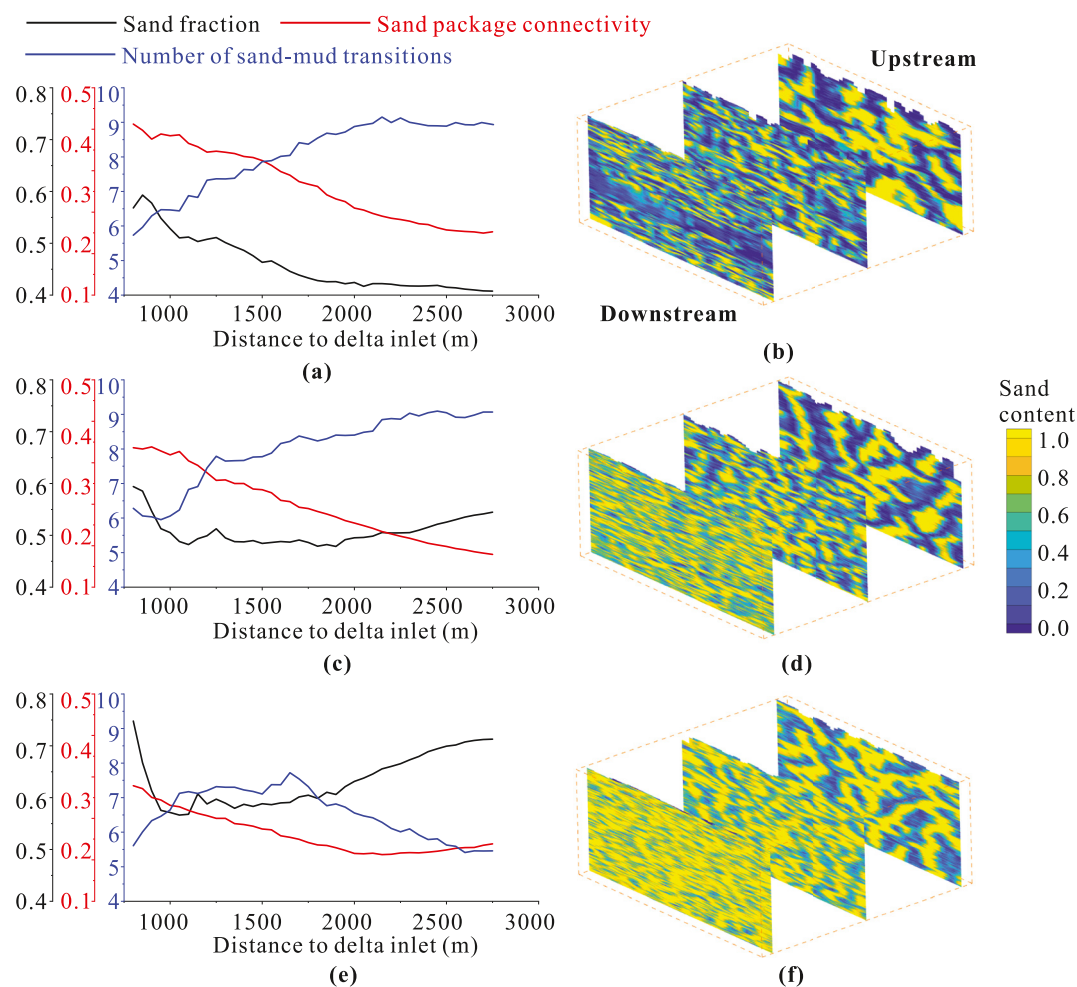


**Figure 11.** Static indicators measured from upstream to downstream in 40 subregions (Figure 10). (a, b) Static indicators and corresponding sediment distribution for 30% input sand fraction (ISF) delta; (c, d) static indicators and corresponding sediment distribution for 50% ISF deltas; (e, f) static indicators and corresponding sediment distribution for 70% ISF deltas. (b), (d), and (f) are a plot of one example among multiple realizations.

Static indicators, including *sand fraction*, *sand package connectivity*, and *number of sand-mud transitions*, vary substantially with ISF, SLR (Figures S2c and S2d in Supporting Information S1), and spatial location (Figure 11). In muddier deltas (30% ISF), more sand accumulates in the upstream, and the *sand fraction* consistently decreases from upstream to downstream (Figure 11a black line and Figure 11b). In sandier deltas (70% ISF), sand tends to accumulate in both upstream and downstream areas (Liang et al., 2016) (Figure 11e black line and Figure 11f) because these rivers transport sufficient sand downstream. *Sand package connectivity* decreases from upstream to downstream in all ISF conditions (Figure 11 red lines). The location of the main channel is more stable than the branches, so the sand distribution in the upstream regions tends to be more vertically connected (Figures 11b, 11d and 11f). The downstream distributaries are more mobile, so sand bodies become thinner (Figures 11b, 11d and 11f). The *number of sand-mud transitions* increases downstream in the 30% and 50% ISF scenarios, showing an inverse behavior with *sand package connectivity* (Figures 11a and 11c). However, for 70% ISF, the *number of sand-mud transitions* decreases with the distance downstream because more sand accumulates in the downstream region (Figure 11e blue line).

The spatial variation in deposition results in different contaminant distributions from upstream to downstream. In 30% and 50% ISF deltas, both the *largest depth* and *average depth of contamination* in widespread surface contamination (Case 1) decrease from upstream to downstream (Figures 12a and 12d black solid and black dotted lines), while the transport depth for 70% ISF decreases first and then increases (Figure 12g black and black dotted lines). This transport behavior follows the *sand fraction* variation (Figures 11a, 11c and 11e black lines). The

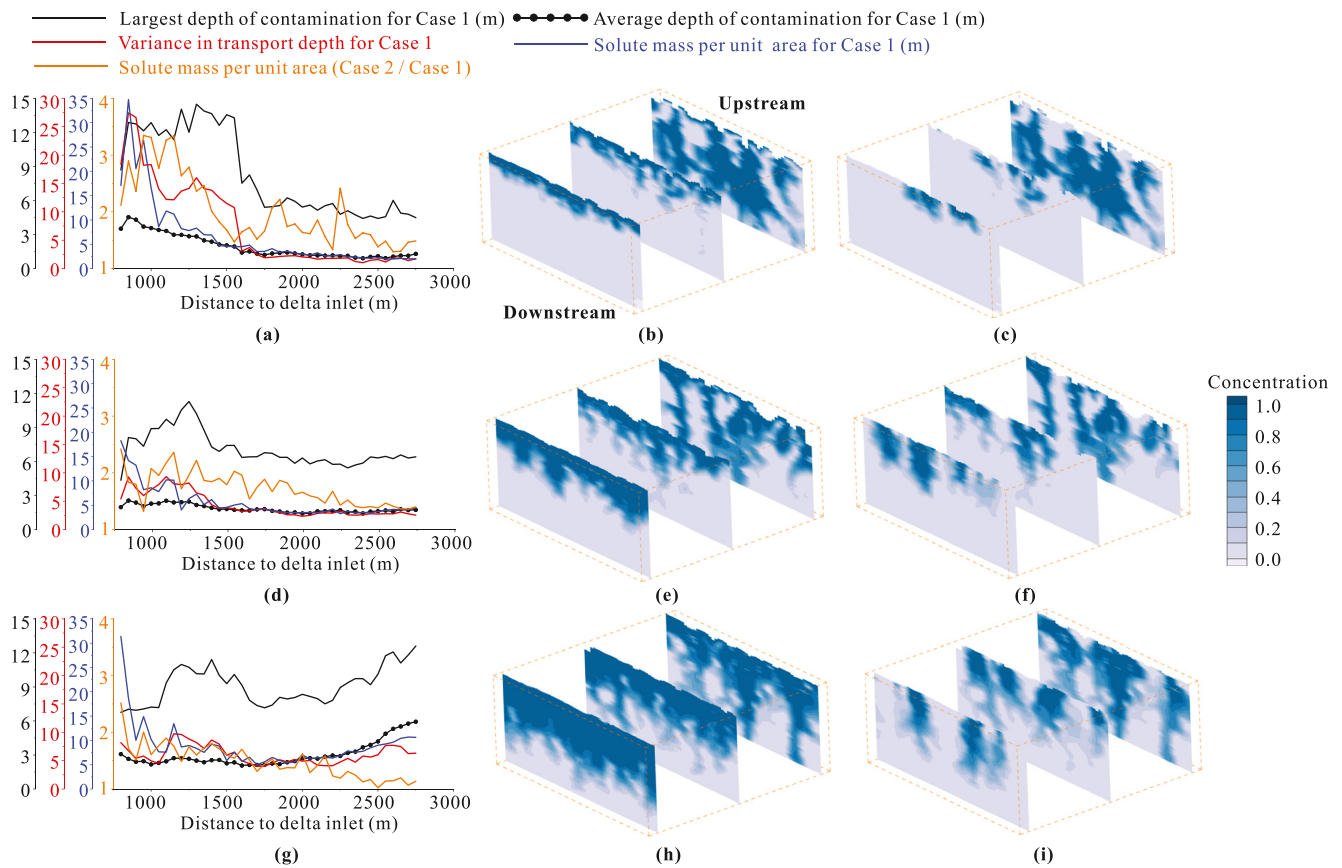


**Figure 12.** Transport metrics measured from upstream to downstream. (a–c) Contamination indicators and corresponding contaminant distribution of Case 1 and Case 2 for 30% input sand fraction (ISF) deltas, respectively; (d–f) contamination indicators and corresponding contaminant distribution of Case 1 and Case 2 for 50% ISF deltas, respectively; (g–i) contamination indicators and corresponding contaminant distribution of Case 1 and Case 2 for 70% ISF deltas, respectively. (b), (c), (e), (f), (h), and (i) Cross-sections of one example among multiple realizations.

*variance in transport depth* (Figures 12a, 12d and 12g red lines) decreases with distance to delta inlet. Upstream channel stacking is stable, generating large sandy patches (Figure 11b, d, f), which are ideal paths for preferential transport (Figures 12b, 12e and 12h). Downstream channels are more mobile and therefore have less consistent stacking patterns, causing lower sand connectivity and lower average contaminant transport depths. The *ratio of solute mass per unit area* (Figures 12a, 12d and 12g brown lines) decreases from upstream to downstream, indicating that the effect of river channels on contaminant transport becomes weaker in the distal zones due to lower connectivity in downstream areas.

### 3.2. Lateral Source of Contamination: Horizontal Transport

**Case 3a.** In the sub-case of steady state salinity distribution and associated density-driven saline groundwater circulation, the *landward position of the interface toe* and the *saline groundwater volume* show that salinity distributions are influenced by ISF (Figures 13a and 13b). Both the *landward position of the interface toe* and *saline groundwater volume* increase rapidly from 30% ISF to 50% ISF, indicating the sandier deltaic aquifers may be more vulnerable to salinization. However, the indicators do not increase substantially from 50% to 70% ISF. This is likely because the sand fraction is already high enough in the 50% ISF scenario that preferential flow is less dominant, so dynamic behaviors are less sensitive to further increases in sand fraction.

*Fresh* and *saline* SGD follow the trend of sand fraction, increasing with higher ISF and decreasing with higher rates of SLR (Figures 13c and 13d, and Figure S2a in Supporting Information S1). For fresh water, this should be primarily controlled by horizontal connectedness and effective  $K$ . More sand leads to a better connection between the inland freshwater boundary and the discharge area, increasing the horizontal effective  $K$ , and the

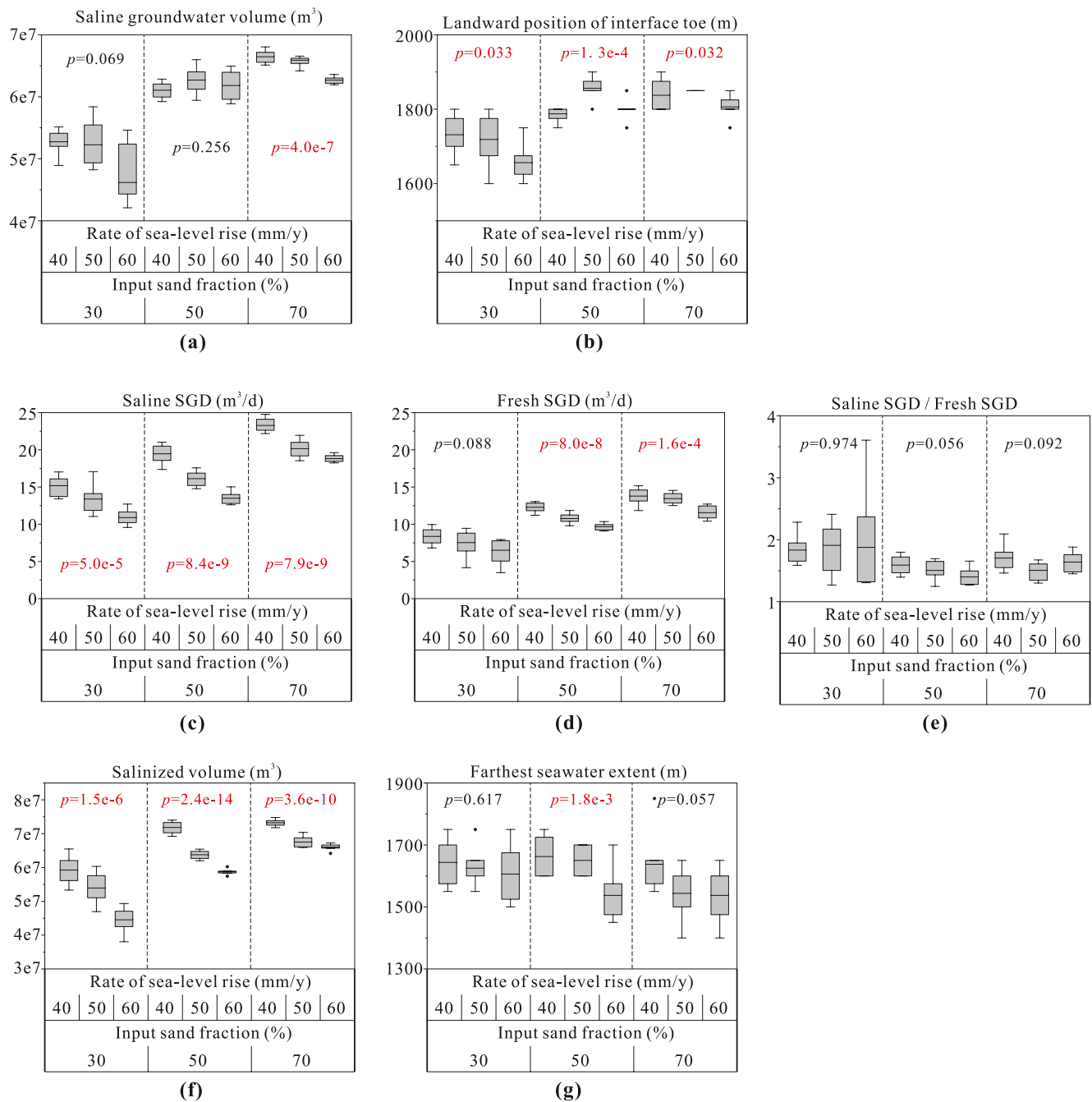


**Figure 13.** Contaminant indicators for Case 3a: (a) Saline groundwater volume, (b) Landward position of interface toe, (c) Saline Submarine groundwater discharge (SGD), (d) Fresh SGD, (e) Saline SGD/Fresh SGD; and Case 3b: (f) Salinized volume, (g) Farthest seawater extent. The  $p$ -values of the Analysis of Variance tests are displayed in each input sand fraction group.  $p$ -Values less than 0.05, shown in red indicate that the differences in transport behavior are statistically significant.

simulated *fresh* SGD nearly linearly increases with horizontal effective  $K$  (Figure S3a and Table S1 in Supporting Information S1). For *saline* SGD, flow is rotational, so it is typically dependent on both horizontal and vertical connectivity and effective  $K$  values. However, the horizontal component dominates in this system, as *saline* SGD correlates nearly linearly with horizontal effective  $K$  and weakly correlates with vertical effective  $K$  (Figure S3b, S3d, and Table S1 in Supporting Information S1). The trends are similar for both *fresh* and *saline* SGD and their ratio does not show a significant trend with ISF or SLR (Figure 13e). There is substantial variability in the ratio for the lowest ISF compared to higher ISF, particularly for higher rates of SLR. The variability is mainly influenced by the sand fraction, as muddier deltas are closer to the system percolation threshold, connectivity

increases dramatically with sand fraction around the threshold (Hunt, 2005; Larue & Hovadik, 2006). Thus, muddier deltas have less-connected structure and preferential flow that leads to higher uncertainty in flow behavior. This also indicates that preferential flow and connectedness play a major role in the relative rates of saline and fresh SGD from coastal aquifers. In addition, all the *ratios of saline to fresh* SGD are larger than 1, a finding that is consistent with simulations in other heterogeneous aquifers (Kreyns et al., 2020; Michael & Khan, 2016); whereas in homogeneous aquifers the ratio is often much less than 1 (Smith, 2004). Furthermore, 73 connectivity metrics of subsurface architecture, flow and transport were used to correlate with the metrics of Case 3a. The correlation shows that horizontal effective  $K$  is the best predictor of salinity distribution and fresh and saline SGD (Text S2 in Supporting Information S1).

**Case 3b.** Lateral movement of seawater into the aquifer due to the sea level higher than the freshwater head is affected by ISF. *Salinized volume* increases from 30% ISF to 50% ISF but is similar between 50% and 70% ISF, (Figure 13f), which is similar to the behavior of *saline groundwater volume* and the *landward position of the interface toe* for the Case 3a (Figures 13a and 13b). The *salinized volume* decreases with SLR, likely due to changes in sand fraction (Figure S2a in Supporting Information S1). The *farthest seawater extent* reflects horizontal preferential transport, which is not systematically affected by external forcings since the models are all highly horizontally connected by sandy paleo-channels (Figure 13g).

## 4. Discussion

Simulations using numerical deltas generated with DeltaRCM under different depositional conditions were run to understand how external forcing affects the vulnerability of deltaic aquifers to contaminant transport. Two external forcings were considered in the model generation: ISF and SLR. Both factors affect sand content within the domain as well as channel distributions and stacking patterns. Higher ISF causes shallower channel deposition and more active channel migration, which results in thinner sand geobodies and thus less vertical connectivity. Higher SLR results in more channel branches, leading to more variable sand distributions in the subsurface. These variations in geologic structure critically affect the contaminant distribution in aquifers.

### 4.1. Implications for Aquifer Vulnerability

Our analysis shows that the vulnerability of deltaic aquifers varies for different contamination sources and flow directions. For widespread surface contamination (Case 1) such as geogenic arsenic contamination, the contaminant distribution is controlled by the total sand fraction and vertical stacking of high-permeability sandy channels. The *average depth of contamination* (Figure 7a) and *solute mass per unit area* (Figure 7b) indicate that sandy aquifers are more vulnerable, and contamination is mainly controlled by ISF. However, the *largest depth of contamination* (Figure 7c) shows that preferential flow can allow solutes to travel quickly even in muddier deltas, indicating that even deltas with low sand content are vulnerable if vertical connections exist.

For surface sources of contamination, the solute distributions vary spatially because the depositional environment affects subsurface features, and the surface channel distributions vary from upstream to downstream. The upstream areas in muddier deltas (Figures 12b and 12e) are more vulnerable to widespread surface contamination than downstream areas because of sand accumulation in the upstream regions. This increases vulnerability to both horizontal and vertical transport, with implications for groundwater management and monitoring in upstream areas. In sandy deltas (Figures 12g and 12h), sand accumulates in both the upstream and downstream areas, increasing vulnerability in the downstream areas relative to downstream areas of muddier deltas. However, in all cases, due to differences in sand distribution, the depth of contamination and its variability in upstream areas are always higher than in downstream areas (Figures 12b, 12e and 12h). Contaminants in the upstream areas tend to move deeper due to rapid flow concentrating in sandy areas of channel stacking. In the downstream areas, lateral channel migration increases, resulting in less vertically connected sand to create preferential transport pathways, thus contaminants in the downstream areas tend to be distributed more widely and evenly. Therefore, groundwater managers may consider different pumping strategies for upstream and downstream areas of sandy deltas. In upstream areas, shallow wells can be used by avoiding localized contamination, whereas in downstream areas, deeper wells may be a better choice for pumping deep, potentially, contaminant-free water. However, deep groundwater downstream may be threatened by seawater intrusion. Therefore, the balance between the pumping depth and pumping distance to the shoreline may need further consideration when multiple sources of contamination are present. The above suggestions are merely based on the general hydrogeologic conditions of deltas.

Site-specific investigations, such as contaminant sampling and detailed numerical models, are still needed to assess specific systems.

When contamination is concentrated in river channels, the potential fast connection to the subsurface results in a contaminant mass in the aquifer disproportionate to the contaminated area on the surface. Because upstream areas have even greater channel connectivity to the subsurface than downstream areas, they may become quickly contaminated during storm events that push brackish water into upstream channels even if they are far from the shoreline (Paldor & Michael, 2021; Yang et al., 2015b; Yu et al., 2016). On the other hand, because there is a close relationship between surface channels and subsurface sandy paleo-channels, the distribution of contaminants may be more easily predicted based on surface features. Particularly in muddier deltas, where less sand input reduces channel mobility and produces more vertical channel stacking, subsurface locations of contaminated water can be inferred from surface channel locations. This finding also applies to cases of widespread surface contamination, because more-preferential transport may occur below surface channel regions. Therefore, groundwater managers may avoid pumping shallow groundwater near rivers, especially in muddier deltas, as the groundwater there may be contaminated by both saline water and preferential transport of arsenic. We note that the surface-to-subsurface channel connectivity does dissipate with depth, so the management strategy of avoiding pumping near rivers would only apply for a depth interval on the order of (perhaps  $\sim 2$  times) the depth of connected sand packages.

All of our simulated deltas are vulnerable to lateral seawater intrusion due to their horizontally connected structure. The paleo-channels are pathways for preferential transport and this high-permeability geologic structure may conduct rapid seawater intrusion under pumping conditions (e.g., Geng & Michael, 2020). Seawater intrudes from the sea to the downstream delta, where the sand distribution is wider and more variable than in the upstream areas. This structure produces multiple preferential flow paths and brings substantial uncertainty to the predictions of contaminant distribution (Text S2 in Supporting Information S1). Managers may seek to avoid pumping water from high-permeability pathways that may induce preferential seawater intrusion. According to our findings, sandy aquifer locations away from rivers are less likely to be part of a paleo-channel connected to the saline part of the aquifer.

#### 4.2. Assumptions and Limitations

This study aims to improve understanding of basic controls on three contamination scenarios in deltaic aquifers with different external forcings during deposition. Several assumptions and simplifications were introduced to make the modeling feasible. First, the rates of SLR used during deposition are unrealistically high. Due to the computational cost, simulation times and memory requirements are high to produce a 30 m-depth delta model under lower SLR conditions. In a previous study (Xu et al., 2021), low-SLR realizations of the subsurface were generated by using a stitching method. The trend in flow behavior from low-SLR to high-SLR simulations was analyzed, and the results showed that the characteristics of flow behavior in low-SLR realizations are predictable from high-SLR models. Horizontal flow connectivity increases with SLR nearly linearly both in low-SLR and high-SLR models, and vertical flow connectivity of low-SLR models is essentially identical to high-SLR realizations (Xu et al., 2021). A second assumption that may affect results is the representation of pumping as an overall vertical hydraulic gradient applied as a consistent boundary condition. In Case 1 and Case 2, pumping effects are simplified as a head difference on boundaries rather than a point water discharge. This set-up approximates the effect of large-scale distributed pumping or a high rate of point pumping from a distal source (see, i.e., Khan et al., 2019; Mozumder et al., 2020). The effect of pumping from individual wells at different rates may be a target for future work. A third simplification is the constant and limited set of forcings simulated during deposition. Real deltas evolved under more complex geologic forcings, such as variable rates of SLR, dynamic sand fraction in sediment transport, and other forcings such as tides or waves. These dynamic forcings may lead to a more complex sediment distribution. The fourth simplification is no delta growth during the flow and transport simulations, despite the comparable time scales of the two processes. Within the scope of this research, it is not possible to fully couple the geomorphological and hydrogeological simulations, and their isolation is still insightful for comparisons between the scenarios discussed here. While the simplified simulations allow us to untangle the effects of individual forcing mechanisms, their combination may be nonlinear, and future work may consider such complexity.

## 5. Conclusion

The security of groundwater quality in deltaic aquifers is critical for hundreds of millions of people living in these environments. This study provides insights into contaminant transport in heterogeneous deltaic aquifers, assesses the vulnerability of different deltas to different sources of contamination, and relates groundwater contamination to the surface-subsurface lithology and depositional environment. Our simulations suggest that different external forcings and spatial locations determine the surface network distribution and subsurface structure, and that structure influences solute transport. Two external forcings were considered, ISF and rate of SLR. Three scenarios of contamination were simulated: widespread surface contamination (Case 1), surface river contamination (Case 2), and lateral seawater intrusion (Case 3).

The main findings are:

1. The coupled effect of sand content and channel stacking determines vertical transport from the entire surface (Case 1). Solute mass and average transport depth increase with ISF, while the largest transport depth does not show a trend with external forcings.
2. For vertical contaminant transport from rivers (Case 2), channel stacking is the primary influence on transport behavior. External forcings have limited effects on Case 2 compared to Case 1, because external forcings have a weaker impact on channel migration than on general system characteristics such as sand fraction.
3. Comparison of Case 1 and Case 2 shows that river channels strongly influence contaminant input due to more connections with sandy channels, and the effect of rivers decreases with increasing sand content.
4. Due to differences in channel migration and sand accumulation, solute transport metrics vary from upstream to downstream.
5. Indicators of steady state salinity distribution (Case 3a) and transient seawater intrusion (Case 3b) approximate trends in sand proportion. The steady state position of the saltwater wedge toe and the volume of saline water significantly increase from 30% to 50% ISF and are similar from 50% to 70% ISF. The greatest inland distance of transient seawater intrusion is not controlled by external forcings under the conditions studied.
6. Groundwater managers may need to use different pumping strategies depending on location within a delta (upstream to downstream) and delta characteristics (sandier vs. muddier). The pumping location is also important, this study suggests that pumping far away from rivers or surface channels could reduce vulnerability to contamination.

Surface-subsurface connectivity is an effective way to predict solute transport in deltas since the processes creating subsurface architecture are also the processes of surface channel evolution. The external forcings, distribution of surface networks, and relative distance to rivers are significant in this prediction. Improving of understanding surface-subsurface water flow and solute transport will improve assessment of the vulnerability of deltaic aquifers to contamination.

## Data Availability Statement

The DeltaRCM model can be downloaded from the CSDMS model repository at <https://github.com/csdms-contrib/DeltaRCM>. Example MODFLOW and MODPATH input files are accessible in CUAHSI Hydroshare (Xu and Michael, 2022).

## References

- Anderson, W. P., Jr. (2002). Aquifer salinization from storm overwash. *Journal of Coastal Research*, 18(3), 413–420. Retrieved from <http://www.jstor.org/stable/4299090>
- Ayers, J. C., Goodbred, S., George, G., Fry, D., Benneyworth, L., Hornberger, G., et al. (2016). Sources of salinity and arsenic in groundwater in southwest Bangladesh. *Geochemical Transactions*, 17(1), 4. <https://doi.org/10.1186/s12932-016-0036-6>
- Bear, J. (1999). *Seawater intrusion in coastal aquifers: Concepts, methods, and practices* (Vol. 14). Kluwer Academic (Theory and applications of transport in porous media).
- Berg, M., Stengel, C., Trang, P. T. K., Viet, P. H., Sampson, M. L., Leng, M., & Fredericks, D. (2007). Magnitude of arsenic pollution in the Mekong and Red River deltas—Cambodia and Vietnam. *Science of the Total Environment*, 372(2–3), 413–425. <https://doi.org/10.1016/j.scitotenv.2006.09.010>
- Berkowitz, B., Scher, H., & Silliman, S. E. (2000). Anomalous transport in laboratory-scale, heterogeneous porous media. *Water Resources Research*, 36(1), 149–158. <https://doi.org/10.1029/1999WR900295>
- Bricheno, L., & Wolf, J. (2018). Modelling tidal river salinity in coastal Bangladesh. In *Ecosystem services for well-being in deltas* (pp. 315–332). Palgrave Macmillan.

## Acknowledgments

We thank the three reviewers and the Associate Editor, whose comments improved the paper. Support for this work was from the National Science Foundation via EAR-1719670 and EAR-1719638.

- Cameo, E. A. (2006). *Seawater intrusion in complex geological environments*. Universitat Politècnica de Catalunya.
- Carrera, J. (1993). An overview of uncertainties in modelling groundwater solute transport. *Journal of Contaminant Hydrology*, *13*(1–4), 23–48. [https://doi.org/10.1016/0169-7722\(93\)90049-X](https://doi.org/10.1016/0169-7722(93)90049-X)
- Edmonds, D. A., Caldwell, R. L., Brondizio, E. S., & Siani, S. M. O. (2020). Coastal flooding will disproportionately impact people on river deltas. *Nature Communications*, *11*(1), 4741. <https://doi.org/10.1038/s41467-020-18531-4>
- Edmonds, D. A., Paola, C., Hoyal, D. C. J. D., & Sheets, B. A. (2011). Quantitative metrics that describe river deltas and their channel networks. *Journal of Geophysical Research*, *116*(F4), F04022. <https://doi.org/10.1029/2010JF001955>
- Erban, L. E., Gorelick, S. M., Zebker, H. A., & Fendorf, S. (2013). Release of arsenic to deep groundwater in the Mekong Delta, Vietnam, linked to pumping-induced land subsidence. *Proceedings of the National Academy of Sciences of the United States of America*, *110*(34), 13751–13756. <https://doi.org/10.1073/pnas.1300503110>
- Feehley, C. E., Zheng, C., & Molz, F. J. (2000). A dual-domain mass transfer approach for modeling solute transport in heterogeneous aquifers: Application to the Macrodispersion Experiment (MADE) site. *Water Resources Research*, *36*(9), 2501–2515. <https://doi.org/10.1029/2000WR900148>
- Fendorf, S., Michael, H. A., & van Geen, A. (2010). Spatial and temporal variations of groundwater arsenic in south and Southeast Asia. *Science*, *328*(5982), 1123–1127. <https://doi.org/10.1126/science.1172974>
- Fiori, A., & Jankovic, I. (2012). On preferential flow, channeling and connectivity in heterogeneous porous formations. *Mathematical Geosciences*, *44*(2), 133–145. <https://doi.org/10.1007/s11004-011-9365-2>
- Geng, X., & Michael, H. A. (2020). Preferential flow enhances pumping-induced saltwater intrusion in volcanic aquifers. *Water Resources Research*, *56*, 5. <https://doi.org/10.1029/2019WR026390>
- Giosan, L., Syvitski, J., Constantinescu, S., & Day, J. (2014). Climate change: Protect the world's deltas. *Nature*, *516*(7529), 31–33. <https://doi.org/10.1038/516031a>
- Harbaugh, A. W. (2005). *MODFLOW-2005, the US geological survey modular groundwater model: The groundwater flow process*. US Department of the Interior, USGS Reston.
- Hariharan, J., Xu, Z., Michael, H. A., Paola, C., Steel, E., & Passalacqua, P. (2021). Linking the surface and subsurface in river deltas - Part 1: Relating surface and subsurface geometries. *Water Resources Research*, *57*(8), e2020WR029282. <https://doi.org/10.1029/2020WR029282>
- Heller, P. L., Paola, C., Hwang, I. G., John, B., & Steel, R. (2001). Geomorphology and sequence stratigraphy due to slow and rapid base-level changes in an experimental subsiding basin (XES 96–1). *AAPG Bulletin*, *85*(5), 817–838. <https://doi.org/10.1306/8626CA0F-173B-11D7-8645000102C1865D>
- Henry, H. R. (1964). *Effects of dispersion on salt encroachment in coastal aquifers* (Vol. 1613-C, pp. 70–84). USGS Water-Supply Paper.
- Hiatt, M., & Passalacqua, P. (2015). Hydrological connectivity in river deltas: The first-order importance of channel-island exchange. *Water Resources Research*, *51*(4), 2264–2282. <https://doi.org/10.1002/2014WR016149>
- Holding, S., & Allen, D. M. (2015). From days to decades: Numerical modelling of freshwater lens response to climate change stressors on small low-lying islands. *Hydrology and Earth System Sciences*, *19*(2), 933–949. <https://doi.org/10.5194/hess-19-933-2015>
- Hoque, M. A., Burgess, W. G., & Ahmed, K. M. (2017). Integration of aquifer geology, groundwater flow and arsenic distribution in deltaic aquifers – A unifying concept. *Hydrological Processes*, *31*(11), 2095–2109. <https://doi.org/10.1002/hyp.11181>
- Hosono, T., Nakano, T., Shimizu, Y., Onodera, S. I., & Taniguchi, M. (2011). Hydrogeological constraint on nitrate and arsenic contamination in Asian metropolitan groundwater. *Hydrological Processes*, *25*(17), 2742–2754. <https://doi.org/10.1002/hyp.8015>
- Hoyal, D. C. J. D., & Sheets, B. A. (2009). Morphodynamic evolution of experimental cohesive deltas. *Journal of Geophysical Research*, *114*(F2), F02009. <https://doi.org/10.1029/2007JF000882>
- Hunt, A. G. (2005). Percolation theory and the future of hydrogeology. *Hydrogeology Journal*, *13*(1), 202–205. <https://doi.org/10.1007/s10040-004-0405-6>
- Kaleris, V. (2006). Submarine groundwater discharge: Effects of hydrogeology and of near shore surface water bodies. *Journal of Hydrology*, *325*(1–4), 1–4. <https://doi.org/10.1016/j.jhydrol.2005.10.008>
- Kerrou, J., & Renard, P. (2009). A numerical analysis of dimensionality and heterogeneity effects on advective dispersive seawater intrusion processes. *Hydrogeology Journal*, *18*(1), 55–72. <https://doi.org/10.1007/s10040-009-0533-0>
- Khan, M. R., Koneshloo, M., Knappett, P. S. K., Ahmed, K. M., Bostick, B. C., Mailloux, B. J., et al. (2016). Megacity pumping and preferential flow threaten groundwater quality. *Nature Communications*, *7*(1), 12833. <https://doi.org/10.1038/ncomms12833>
- Khan, M. R., Michael, H. A., Nath, B., Huhmann, B. L., Harvey, C. F., Mukherjee, A., et al. (2019). High-arsenic groundwater in the southwestern Bengal Basin caused by a lithologically controlled deep flow system. *Geophysical Research Letters*, *46*(22), 13062–13071. <https://doi.org/10.1029/2019GL084767>
- Knudby, C., & Carrera, J. (2005). On the relationship between indicators of geostatistical, flow and transport connectivity. *Advances in Water Resources*, *28*(4), 405–421. <https://doi.org/10.1016/j.advwatres.2004.09.001>
- Kolker, A. S., Cable, J. E., Johannesson, K. H., Allison, M. A., & Inness, L. V. (2013). Pathways and processes associated with the transport of groundwater in deltaic systems. *Journal of Hydrology*, *498*, 319–334. <https://doi.org/10.1016/j.jhydrol.2013.06.014>
- Kreyns, P., Geng, X., & Michael, H. A. (2020). The influence of connected heterogeneity on groundwater flow and salinity distribution in a coastal volcanic aquifer. *Journal of Hydrology*, *586*, 124863. <https://doi.org/10.1016/j.jhydrol.2020.124863>
- Langevin, C. D., Thorne, D. T., Dausman, A. M., Sukop, M. C., & Guo, W. (2008). *SEAWAT version 4: A computer program for simulation of multi-species solute and heat transport*. U.S. Geological Survey Techniques and Methods Book (Vol. 6, No. (A22), p. 39).
- Larue, D. K., & Hovadik, J. (2006). Connectivity of channelized reservoirs: A modelling approach. *Petroleum Geoscience*, *12*(4), 291–308. <https://doi.org/10.1144/1354-079306-699>
- Le Goc, R., de Dreuzy, J. R., & Davy, P. (2010). Statistical characteristics of flow as indicators of channeling in heterogeneous porous and fractured media. *Advances in Water Resources*, *33*(3), 257–269. <https://doi.org/10.1016/j.advwatres.2009.12.002>
- Liang, M., Dyk, C. V., & Passalacqua, P. (2016). Quantifying the patterns and dynamics of river deltas under conditions of steady forcing and relative sea level rise. *Journal of Geophysical Research: Earth Surface*, *121*(2), 465–496. <https://doi.org/10.1002/2015JF003653>
- Liang, M., Voller, V. R., & Paola, C. (2015). A reduced-complexity model for river delta formation - Part 1: Modeling deltas with channel dynamics. *Earth Surface Dynamics*, *3*(1), 67–86. <https://doi.org/10.5194/esurf-3-67-2015>
- Lu, C., Chen, Y., Zhang, C., & Luo, J. (2013). Steady-state freshwater–seawater mixing zone in stratified coastal aquifers. *Journal of Hydrology*, *505*, 24–34. <https://doi.org/10.1016/j.jhydrol.2013.09.017>
- Michael, H. A., & Khan, M. R. (2016). Impacts of physical and chemical aquifer heterogeneity on basin-scale solute transport: Vulnerability of deep groundwater to arsenic contamination in Bangladesh. *Advances in Water Resources*, *98*, 147–158. <https://doi.org/10.1016/j.advwatres.2016.10.010>

- Michael, H. A., Russoniello, C. J., & Byron, L. A. (2013). Global assessment of vulnerability to sea-level rise in topography-limited and recharge-limited coastal groundwater systems. *Water Resources Research*, 49(4), 2228–2240. <https://doi.org/10.1002/wrcr.20213>
- Michael, H. A., Scott, K. C., Koneshloo, M., Yu, X., Khan, M. R., & Li, K. (2016). Geologic influence on groundwater salinity drives large seawater circulation through the continental shelf. *Geophysical Research Letters*, 43, <https://doi.org/10.1002/2016GL070863>
- Michael, H. A., & Voss, C. I. (2008). Evaluation of the sustainability of deep groundwater as an arsenic-safe resource in the Bengal Basin. *Proceedings of the National Academy of Sciences of the United States of America*, 105(25), 8531–8536. <https://doi.org/10.1073/pnas.0710477105>
- Mozumder, M. R. H., Michael, H. A., Mihajlov, I., Khan, M. R., Knappett, P. S. K., Bostick, B. C., et al. (2020). Origin of groundwater arsenic in a rural Pleistocene aquifer in Bangladesh depressurized by distal municipal pumping. *Water Resources Research*, 55(7), e2020WR027178. <https://doi.org/10.1029/2020WR027178>
- Mulligan, A. E., Evans, R. L., & Lizarralde, D. (2007). The role of paleochannels in groundwater/seawater exchange. *Journal of Hydrology*, 335(3–4), 313–329. <https://doi.org/10.1016/j.jhydrol.2006.11.025>
- Ng, J. C., Wang, J., & Shraim, A. (2003). A global health problem caused by arsenic from natural sources. *Chemosphere*, 52(9), 1353–1359. [https://doi.org/10.1016/S0045-6535\(03\)00470-3](https://doi.org/10.1016/S0045-6535(03)00470-3)
- Nofal, E., Amer, M., El-Didy, S., & Fekry, A. M. (2015). Sea water intrusion in Nile Delta in perspective of new configuration of the aquifer heterogeneity using the recent stratigraphy data. *Journal of American Science*, 11(6), 281–292.
- Paldor, A., & Michael, H. A. (2021). Storm surges cause simultaneous salinization and freshening of coastal aquifers, exacerbated by climate change. *Water Resources Research*, 57(5), e2020WR029213. <https://doi.org/10.1029/2020WR029213>
- Radloff, K. A., Zheng, Y., Michael, H. A., Stute, M., Bostick, B. C., Mihajlov, I., et al. (2011). Arsenic migration to deep groundwater in Bangladesh influenced by adsorption and water demand. *Nature Geoscience*, 4(11), 793–798. <https://doi.org/10.1038/NGEO1283>
- Rao, S. V. N., Bhallamudi, S. M., Thandaveswara, B. S., & Sreenivasulu, V. (2005). Planning groundwater development in coastal deltas with paleo channels. *Water Resources Management*, 19(5), 625–639. <https://doi.org/10.1007/s11269-005-5604-y>
- Reitz, M. D., Pickering, J. L., Goodbred, S. L., Paola, C., Steckler, M. S., Seeber, L., & Akhter, S. H. (2015). Effects of tectonic deformation and sea level on river path selection: Theory and application to the Ganges-Brahmaputra-Meghna River Delta. *Journal of Geophysical Research: Earth Surface*, 120(4), 671–689. <https://doi.org/10.1002/2014JF003202>
- Renard, P., & Allard, D. (2013). Connectivity metrics for subsurface flow and transport. *Advances in Water Resources*, 51, 168–196. <https://doi.org/10.1016/j.advwatres.2011.12.001>
- Rubin, Y. (1991). Transport in heterogeneous porous media: Prediction and uncertainty. *Water Resources Research*, 27(7), 1723–1738. <https://doi.org/10.1029/91WR00589>
- Sawyer, A. H., Edmonds, D. A., & Knights, D. (2015). Surface water-groundwater connectivity in deltaic distributary channel networks. *Geophysical Research Letters*, 42(10), 10299–10306. <https://doi.org/10.1002/2015GL066156>
- Sebben, M. L., Werner, A. D., & Graf, T. (2015). Seawater intrusion in fractured coastal aquifers: A preliminary numerical investigation using a fractured Henry problem. *Advances in Water Resources*, 85, 93–108. <https://doi.org/10.1016/j.advwatres.2015.09.013>
- Shammi, M., Rahman, M. M., Bondad, S. E., & Bodrud-Doza, M. (2019). Impacts of salinity intrusion in community health: A review of experiences on drinking water sodium from coastal areas of Bangladesh. In *Healthcare (Basel)* (Vol. 7, No. (1), p. 50). MDPI. <https://doi.org/10.3390/healthcare7010050>
- Shamsudduha, M., Taylor, R. G., Ahmed, K. M., & Zahid, A. (2011). The impact of intensive groundwater abstraction on recharge to a shallow regional aquifer system: Evidence from Bangladesh. *Hydrogeology Journal*, 19(4), 901–916. <https://doi.org/10.1007/s10040-011-0723-4>
- Shaw, J. B. (2013). *The kinematics of distributary channels on the Wax Lake Delta, coastal Louisiana, USA* (Doctoral dissertation). The University of Texas at Austin.
- Sheets, B. A., Hickson, T. A., & Paola, C. (2002). Assembling the stratigraphic record: Depositional patterns and time-scales in an experimental alluvial basin. *Basin Research*, 14(3), 287–301. <https://doi.org/10.1046/j.1365-2117.2002.00185.x>
- Smith, A. J. (2004). Mixed convection and density-dependent seawater circulation in coastal aquifers. *Water Resources Research*, 40(8), W08309. <https://doi.org/10.1029/2003WR002977>
- Syvitski, J. P. M., & Saito, Y. (2007). Morphodynamics of deltas under the influence of humans. *Global and Planetary Change*, 57(3–4), 261–282. <https://doi.org/10.1016/j.gloplacha.2006.12.001>
- Taylor, R. G., Scanlon, B., Doll, P., Rodell, M., van Beek, R., Wada, Y., et al. (2013). Ground water and climate change. *Nature Climate Change*, 3(4), 322–329. <https://doi.org/10.1038/nclimate1744>
- Vetrimurugan, E., Elango, L., & Rajmohan, N. (2013). Sources of contaminants and groundwater quality in the coastal part of a river delta. *International Journal of Environmental Science and Technology*, 10(3), 473–486. <https://doi.org/10.1007/s13762-012-0138-3>
- Vithanage, M., Engesgaard, P., Jensen, K. H., Illangasekare, T. H., & Obeysekera, J. (2012). Laboratory investigations of the effects of geologic heterogeneity on groundwater salinization and flush-out times from a tsunami-like event. *Journal of Contaminant Hydrology*, 136–137, 10–24. <https://doi.org/10.1016/j.jconhyd.2012.05.001>
- Wen, X. H., & Gomez-Hernandez, J. J. (1998). Numerical modeling of macro-dispersion in heterogeneous media - A comparison of multi-Gaussian and non-multi-Gaussian models. *Journal of Contaminant Hydrology*, 30(1–2), 129–156. [https://doi.org/10.1016/S0169-7722\(97\)00035-1](https://doi.org/10.1016/S0169-7722(97)00035-1)
- Werner, A. D., Bakker, M., Post, V. E. A., Vandenbohede, A., Lu, C., Ataie-Ashtiani, B., et al. (2013). Seawater intrusion processes, investigation and management: Recent advances and future challenges. *Advances in Water Resources*, 51, 3–26. <https://doi.org/10.1016/j.advwatres.2012.03.004>
- Werner, A. D., & Simmons, C. T. (2009). Impact of sea-level rise on seawater intrusion in coastal aquifers. *Ground Water*, 47(2), 197–204. <https://doi.org/10.1111/j.1745-6584.2008.00535.x>
- Western, A. W., Blöschl, G., & Grayso, R. B. (2001). Toward capturing hydrologically significant connectivity in spatial patterns. *Water Resources Research*, 37(1), 83–97. <https://doi.org/10.1029/2000WR900241>
- WHO. (2011). *Arsenic in drinking-water: Background document for development of WHO guidelines for drinking-water quality*. World Health Organization. IWHO/SDE/WSH/03.04/75/Rev/1. <https://doi.org/10.1016/j.kjms.2011.05.002>
- Xu, Z., Hariharan, J., Passalacqua, P., Elisabeth, S., Paola, C., & Michael, H. A. (2021). Linking the surface and subsurface in river deltas - Part 2: Relating subsurface geometry to groundwater flow behavior. *Water Resources Research*, 57(8), e2020WR029281. <https://doi.org/10.1029/2020WR029281>
- Xu, Z., Hu, B. X., Xu, Z., & Wu, X. (2019). Numerical study of groundwater flow cycling controlled by seawater/freshwater interaction in Woodville Karst Plain. *Journal of Hydrology*, 579, 124171. <https://doi.org/10.1016/j.jhydrol.2019.124171>
- Yang, J., Graf, T., & Ptak, T. (2015a). Impact of climate change on freshwater resources in a heterogeneous coastal aquifer of Bremerhaven, Germany: A three-dimensional modeling study. *Journal of Contaminant Hydrology*, 177(178), 107–121. <https://doi.org/10.1016/j.jconhyd.2015.03.014>

- Yang, J., Graf, T., & Ptak, T. (2015b). Sea level rise and storm surge effects in a coastal heterogeneous aquifer: A 2D modelling study in Northern Germany. *Grundwasser*, 20(1), 39–51. <https://doi.org/10.1007/s00767-014-0279-z>
- Yang, J., Zhang, H., Yu, X., Graf, T., & Michael, H. A. (2018). Impact of hydrogeological factors on groundwater salinization due to ocean surge inundation. *Advances in Water Resources*, 111, 423–434. <https://doi.org/10.1016/j.advwatres.2017.11.017>
- Yu, W. (2010). *Implications of climate change for fresh groundwater resources in coastal aquifers in Bangladesh*. World Bank.
- Yu, X., & Michael, H. A. (2019). Mechanisms, configuration typology, and vulnerability of pumping-induced seawater intrusion in heterogeneous aquifers. *Advances in Water Resources*, 128, 117–128. <https://doi.org/10.1016/j.advwatres.2019.04.013>
- Yu, X., Yang, J., Graf, T., Koneshloo, M., O'Neal, M. A., & Michael, H. A. (2016). Impact of topography on groundwater salinization due to ocean surge inundation. *Water Resources Research*, 52(8), 5794–5812. <https://doi.org/10.1002/2016WR018814>
- Zheng, C., & Wang, P. P. (1999). *MT3DMS: A modular three-dimensional multispecies transport model for simulation of advection, dispersion, and chemical reactions of contaminants in groundwater systems; documentation and user's guide*. DTIC Document.
- Zinn, B., & Harvey, C. F. (2003). When good statistical models of aquifer heterogeneity go bad: A comparison of flow, dispersion, and mass transfer in connected and multivariate Gaussian hydraulic conductivity fields. *Water Resources Research*, 39(3), 1051. <https://doi.org/10.1029/2001WR001146>